Korean J. Chem. Eng., 36(5), 807-815 (2019)
DOI: 10.1007/s11814-019-0258-2

pISSN: 0256-1115
eISSN: 1975-7220

Heterostructured $Co_{0.5}Mn_{0.5}Fe_2O_4$-polyaniline nanofibers: highly efficient photocatalysis for photodegradation of methyl orange

Hong-Ryun Jung*, Kyung Nam Kim, and Wan-Jin Lee*,†**

*School of Chemical Engineering, Chonnam National University, Gwangju 61186, Korea
**Department of Chemical and Environmental Engineering, Sehan University, Jeonnam 58447, Korea
(*Received 30 January 2019 • accepted 26 March 2019*)

Abstract−1D hollow $Co_{0.5}Mn_{0.5}Fe_2O_4$-PANI nanofibers were synthesized through sequential processes of electrospinning, heat treatment in air, and chemical polymerization of polyaniline. The morphology and photocatalytic properties of heterostructured $Co_{0.5}Mn_{0.5}Fe_2O_4$-PANI as photocatalysts were investigated by SEM, TEM, XRD, TGA, and photocatalysis experiments of methyl orange under visible-light irradiation. The hollow $Co_{0.5}Mn_{0.5}Fe_2O_4$-PANI nanofibers showed a high photocatalytic degradation efficiency of 92% within 120 min and a kinetic constant of 115-times higher than hollow $Co_{0.5}Mn_{0.5}Fe_2O_4$ nanofibers. These high photocatalytic properties are attributed to both unique 1D hollow nanofiber morphology with macroporous hollow core, PANI/$Co_{0.5}Mn_{0.5}Fe_2O_4$/PANI shell and the heterojunction structure composed of $Co_{0.5}Mn_{0.5}Fe_2O_4$ and PANI. In addition, the outstanding magnetic properties of the hollow $Co_{0.5}Mn_{0.5}Fe_2O_4$-PANI nanofibers with its inherent spinel structure facilitate the recovery of the photocatalyst.

Keywords: Hollow-structured, Heterojunction, Photocatalytic, Magnetically Separable, Electrospinning

INTRODUCTION

Spinel ferrites (AFe_2O_4, A=Co, Mn, Ni, Zn, Cu) have been studied as promising photocatalysts for photolysis due to their excellent photochemical stability, high recovery rate, and small bandgap (~2 eV) [1-5]. Having metal cations in tetrahedral A and octahedron B sites, they are notable candidates as photocatalyst because it is easy to manipulate the electrical, magnetic and structural properties according to appropriate distribution of the metal cations [6,7]. Especially, the study on the mixing of Co and Mn cations with different ionic radii in the spinel ferrites has been carried out steadily until now because it leads to the modifications relating to the magnetic properties such as coercivity and magnetization as well as morphology change like particle size and crystallinity [8-12]. The behavior of photocatalyst for $Co_{0.5}Mn_{0.5}Fe_2O_4$ as the combination of $[Co^{2+}]_{0.5}$ and $[Mn^{2+}]_{0.5}$ coexistent in spinel structure could be a meaningful milestone for the enhancement of photodegradation efficiency.

The heterostructured $Co_{0.5}Mn_{0.5}Fe_2O_4$-conducting polymer composites with one-dimensional nanostructure have been recently required for magnetically separable photocatalyst suitable for both photocatalytic activity and photocatalyst recovery under UV and visible light. The 1D heterostructured nanofiber composites in the view of photocatalytic activity possess abundant catalytic active sites and delocalized electron by generating the space charge region along the length direction, resulting in remarkably reducing the recombination probability of electron-hole pairs [13]. To this issue, it is essential to design one-dimensional magnetic photocatalyst as nanostructured hybrid system easily absorbable for incident beam. Electrospinning fabricating nanofibers using an electric field is an efficient technique to make well-oriented hollow fiber with high surface area included with volume ratio and large aspect ratio, which is obtained from the composite solution through nearly homogeneous mixing between the polymer solution and the metal precursors [14-21].

A novel design of highly porous heterostructured hollow ferrite-conducting polymer nanofibers is deeply dependent on the materialization of excellent photocatalytic activity and exceptional photocatalyst recovery. The polyaniline (PANI) as a conducting polymer is a favorable sensitizer due to its conjugated electron system with delocalized conjugated structure, which results in fast photoinduced charge separation as well as sluggish charge recombination by high absorption under visible-light. In addition, the positively charged PANI back bone by doping induces interaction with the methyl orange (MO) dye, resulting in high adsorption of the dye [22-26].

As a result, electrospun $Co_{0.5}Mn_{0.5}Fe_2O_4$ hollow nanofibers coated with polyaniline ($Co_{0.5}Mn_{0.5}Fe_2O_4$-PANI) offer exceptional photocatalysis as well as marvelous recovery of photocatalysts as follows: 1) 1D hollow nanofibers with surface area and a large aspect ratio provide a facile pathway of electron transfer, the effect of quantum confinement, and easy absorption of incident beam. 2) $Co_{0.5}Mn_{0.5}Fe_2O_4$-PANI has the advantage of fast mass transfer, resulting in easy adsorption of MO dyes caused by the positively charged PANI coated on the inner and outer surfaces of the hollow nanofiber. 3) PANI as a photosensitizer promotes the utilization of light by easily separating electrons and holes in the visible region. 4) Heterostructured hollow $Co_{0.5}Mn_{0.5}Fe_2O_4$-PANI nanofibers prevent the recombination of the photogenerated carrier and actualize the excellent recovery rate of the photocatalyst after photodegradation due to the inherent properties of spinel ferrites [22,27].

Herein, we report on the first preparation of 1D hollow $Co_{0.5}Mn_{0.5}Fe_2O_4$-PANI nanofibers with excellent visible-light photodegrada-

†To whom correspondence should be addressed.
E-mail: wjlee@jnu.ac.kr

tion of MO dye and remarkable recovery as a magnetically separable photocatalyst. Hollow $Co_{0.5}Mn_{0.5}Fe_2O_4$-PANI nanofibers with high surface area generated with highly macroporous and mesoporous morphology induce the effects of quantum confinement, easily harvest visible light, promote charge separation, and facilitate electron transfer and mass transfer. Although 1D hollow $Co_{0.5}Mn_{0.5}Fe_2O_4$ nanofibers alone are inactive under visible-light irradiation, heterojunction of $Co_{0.5}Mn_{0.5}Fe_2O_4$ and PANI generates notable photodegradation of MO dye.

MATERIALS AND METHODS

1. Preparation of Hollow $Co_{0.5}Mn_{0.5}Fe_2O_4$-PANI Nanofiber

The polymer solution was prepared by dissolving 1.2 g polyvinylpyrrolidone (PVP: Mw 1,300,000) with 8.6 g ethanol and 5.4 g water for 1 h at 80 °C. After that, the composite solution was prepared by mixing the polymer solution with 0.28 g $Co(NO_3)_2{\cdot}6H_2O$, 0.25 g $Mn(NO_3)_2{\cdot}4H_2O$ and 1.45 g $Fe(NO_3)_3{\cdot}9H_2O$ for 12 h at room temperature. Electrospinning was conducted by using the syringe inserted with 10 ml composite solution in the condition of 20 kV applied voltage, 17 cm distance of needle tip to collector, and 0.5 ml h^{-1} flow rate, and then electrospun nanofibers were dried for 24 h at 80 °C. Hollow $Co_{0.5}Mn_{0.5}Fe_2O_4$ nanofibers were prepared by calcining dried electrospun nanofibers at 550 °C for 2 h after elevating at a heating rate of 5 °C min^{-1} in air. Hollow nanofibers were formed by selectively removing PVP in the process of calcination. Hollow $Co_{0.5}Mn_{0.5}Fe_2O_4$-PANI nanofibers were prepared by chemically polymerizing PANI onto the surface of hollow $Co_{0.5}Mn_{0.5}Fe_2O_4$ nanofibers as follows. 0.5 g $Co_{0.5}Mn_{0.5}Fe_2O_4$ nanofibers were well-dispersed into the beaker in 80 mL deionized water and 20 mL HCl solution (1 M), added 1.225 g $(NH_4)_2S_2O_8$, and then sonicated for 1 hr. Afterwards, 0.5 mL aniline was put into the above mixture in an ice-water bath under continuous stirring, and chemically oxidative polymerization was conducted for 6 h. The obtained hollow $Co_{0.5}Mn_{0.5}Fe_2O_4$-PANI nanofibers were rinsed in deionized water several times, and then dried at 70 °C for 12 h.

2. Characterization of Hollow $Co_{0.5}Mn_{0.5}Fe_2O_4$ and $Co_{0.5}Mn_{0.5}Fe_2O_4$-PANI Nanofibers

The morphology of the hollow $Co_{0.5}Mn_{0.5}Fe_2O_4$ and $Co_{0.5}Mn_{0.5}Fe_2O_4$-PANI nanofibers was characterized using a field emission scanning electron microscope (FE-SEM) (Hitachi, S-4700, Japan). The hollow structure and crystalline size of $Co_{0.5}Mn_{0.5}Fe_2O_4$ and hollow $Co_{0.5}Mn_{0.5}Fe_2O_4$-PANI nanofibers were observed by using transmission electron microscope (TEM) (JEOL, JEM-2000 FXII, USA). The weight loss of the hollow $Co_{0.5}Mn_{0.5}Fe_2O_4$, and $Co_{0.5}Mn_{0.5}Fe_2O_4$-PANI nanofibers was measured by thermogravimetric analysis (TGA) (Shi-madzu, TA-50, Japan). The crystal structure of $Co_{0.5}Mn_{0.5}Fe_2O_4$, and $Co_{0.5}Mn_{0.5}Fe_2O_4$-PANI was investigated by X-ray diffraction (XRD) (Rigaku, D/MAX Ultima III, Japan). The surface and pore characteristics were verified using the nitrogen sorption isotherms (condition: 77 K, Micromeritics, ASAP 2020, USA). The pore characteristics such as specific surface area and pore size distribution of the photocatalysts were determined according to the methods of the BET and BJH. The optical absorption of

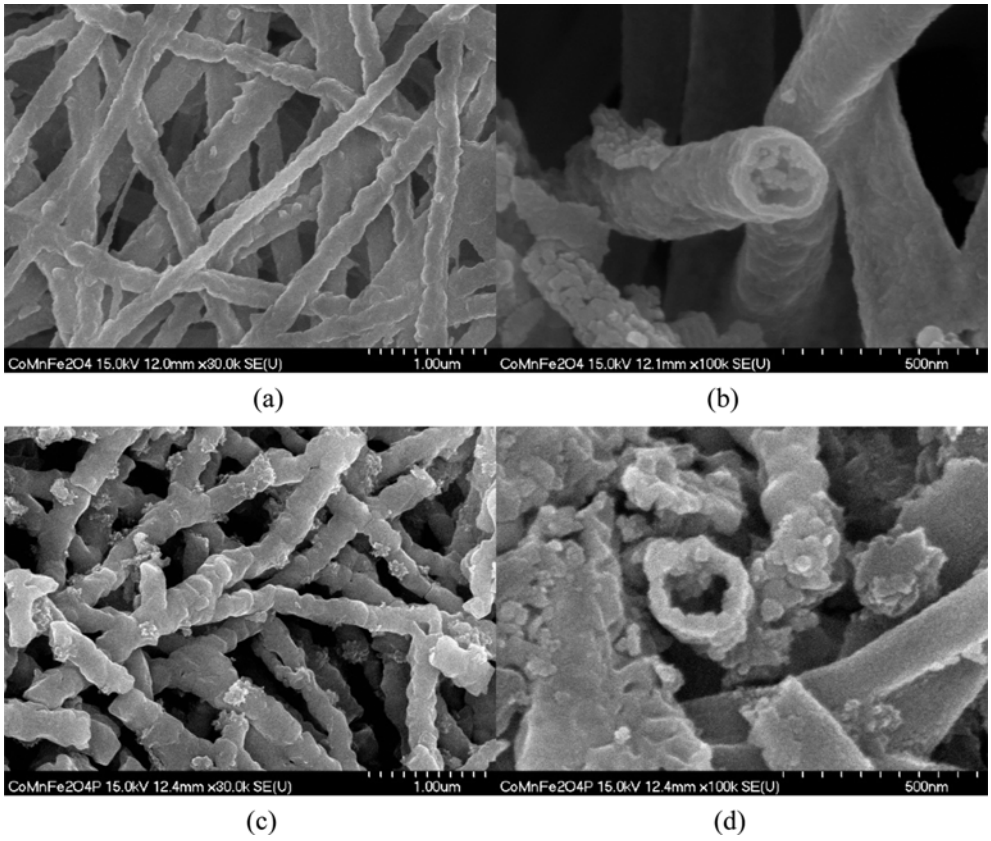

Fig. 1. SEM images (a), (b) as-prepared hollow $Co_{0.5}Mn_{0.5}Fe_2O_4$ nanofibers and (c), (d) $Co_{0.5}Mn_{0.5}Fe_2O_4$-PANI nanofibers.

$Co_{0.5}Mn_{0.5}Fe_2O_4$ and $Co_{0.5}Mn_{0.5}Fe_2O_4$-PANI nanofibers as photocatalysts was investigated using Shimadzu 2600 UV-vis spectrophotometer under 300-800 nm wavelength range.

3. Photocatalytic Degradation of Methyl Orange

Photocatalytic activity was estimated by methyl orange (MO) photodegradation under visible-light irradiation (10 W LED lamp: Seoul Semiconductor Co., 6500 K). The initial MO concentration was 0.02 g L^{-1}. 0.02 g photocatalyst was put into 100 mL MO aqueous solution, and then 4 mL sample was collected according to interval time. The photodegradation efficiency for MO was calculated as follows: $\eta=\{1-C/C_o\}$, where η is the photodegradation efficiency, and both C_o and C are the initial concentration and the concentration at time (t), respectively.

RESULTS AND DISCUSSION

1. Morphology of Hollow $Co_{0.5}Mn_{0.5}Fe_2O_4$ and $Co_{0.5}Mn_{0.5}Fe_2O_4$-PANI Nanofibers

The SEM images of hollow $Co_{0.5}Mn_{0.5}Fe_2O_4$ nanofibers after calcining electrospun PVP/$Co_{0.5}Mn_{0.5}Fe_2O_4$ precursor at 550 °C are shown in Fig. 1(a) and (b). The $Co_{0.5}Mn_{0.5}Fe_2O_4$ nanofibers consist of 1D hollow-structured nanofibers with rough and shrunken surface due to the PVP decomposition as a template during calcination. The cross sections of $Co_{0.5}Mn_{0.5}Fe_2O_4$ nanofibers obviously show the hollow morphology. Hollow $Co_{0.5}Mn_{0.5}Fe_2O_4$ nanofibers with an average diameter of 220 nm are composed of hollow core thickness of 175 nm and shell thickness of 23 nm. Hollow cores of nanofibers and spaces between interconnected nanofibers represent macroporous structure, while the shells display mesoporous structure and improve mass transfer by capillary force formed between interparticles. Fig. 1(c) and (d) illustrate the SEM images of hollow $Co_{0.5}Mn_{0.5}Fe_2O_4$-PANI nanofibers. The PANI granules are coated well on the entire surface of hollow $Co_{0.5}Mn_{0.5}Fe_2O_4$ nanofibers, resulting in thicker hollow $Co_{0.5}Mn_{0.5}Fe_2O_4$-PANI nanofibers of 270 nm in average diameter. Fig. 1(c) and (d) show the obvious void space inside the $Co_{0.5}Mn_{0.5}Fe_2O_4$ nanofiber and the PANI well-coated with the inner- and outer shell. One-dimensional (1D) hollow nanofibers, which are covered with PANI granules, facilitate

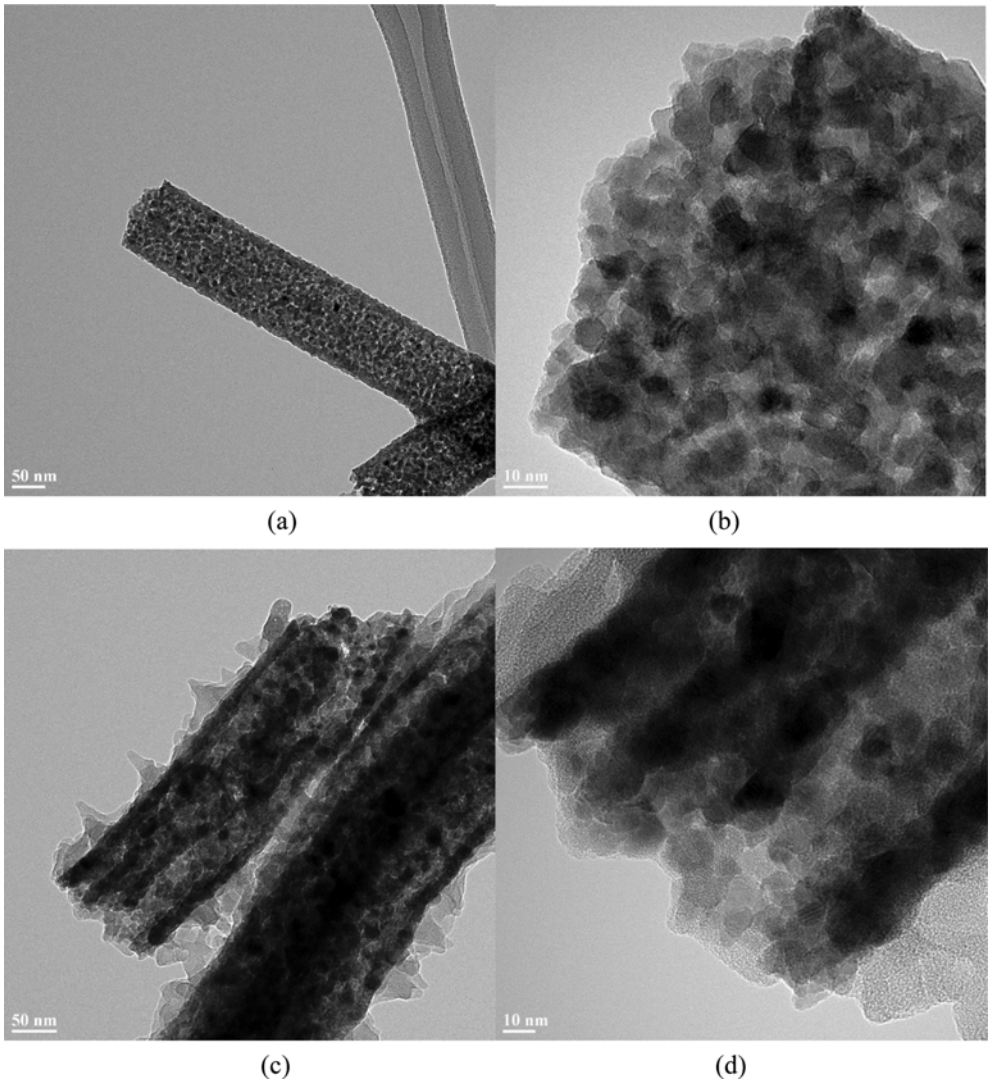

Fig. 2. TEM images for (a), (b) hollow $Co_{0.5}Mn_{0.5}Fe_2O_4$ nanofibers and (c), (d) $Co_{0.5}Mn_{0.5}Fe_2O_4$-PANI nanofibers.

photocatalytic degradation, due to the enhanced electrical conductivity and the better optical characteristics by easily harvesting the visible light. The TEM images of hollow $Co_{0.5}Mn_{0.5}Fe_2O_4$ nanofibers at low magnification and high magnification are illustrated in Fig. 2(a) and (b). The hollow fibers are clearly distinguished as the macroporous hollow and mesoporous shells by contrasting the differences of image. The $Co_{0.5}Mn_{0.5}Fe_2O_4$ shells consist of numerous particles of approximately 7 nm in mean particle size suitable for the photocatalytic quantum confinement effect. Fig. 2(c) and 2(d) show TEM images of 1D hollow $Co_{0.5}Mn_{0.5}Fe_2O_4$-PANI nanofibers photographed with low and high magnification. The 1D hollow-structured $Co_{0.5}Mn_{0.5}Fe_2O_4$ nanofibers are composed of the macroporous hollow core and the mesoporous $Co_{0.5}Mn_{0.5}Fe_2O_4$ shell with amorphous PANI. The boundary between the interior hollow core and the shell is distinct from the difference of the contrast. Fig. 2(c) and (d) show that the $Co_{0.5}Mn_{0.5}Fe_2O_4$ shell stacked with nanoparticles is well-arranged along radial axis of the fiber, representing its shell thickness of ~23 nm. Amorphous PANI also is well-coated on the surface of 1D hollow $Co_{0.5}Mn_{0.5}Fe_2O_4$ nanofiber, showing the PANI thickness of 25 nm. Consequently, the 1D hollow $Co_{0.5}Mn_{0.5}Fe_2O_4$ nanofibers prepared by electrospinning and PANI polymerization are composed of a three-layer PANI/$Co_{0.5}Mn_{0.5}Fe_2O_4$/PANI shell.

2. Crystal Structure of Hollow $Co_{0.5}Mn_{0.5}Fe_2O_4$ and $Co_{0.5}Mn_{0.5}Fe_2O_4$-PANI Nanofibers

The XRD diffraction patterns of hollow $Co_{0.5}Mn_{0.5}Fe_2O_4$ and $Co_{0.5}Mn_{0.5}Fe_2O_4$-PANI nanofibers are shown in Fig. 3. The XRD patterns of single-phase $Co_{0.5}Mn_{0.5}Fe_2O_4$ crystalline are matched as the combination of those of $CoFe_2O_4$ (JCPDS No. 22-1086) and $MnFe_2O_4$ (JCPDS 10-0319). The strong diffraction peaks at 2θ= 18.2°, 30.2°, 35.5°, 36.2°, 43.3°, 53.5° and 57.3°, 62.7°, 73.2° correspond to (111), (220), (311), (222), (400), (422) and (511), (440),

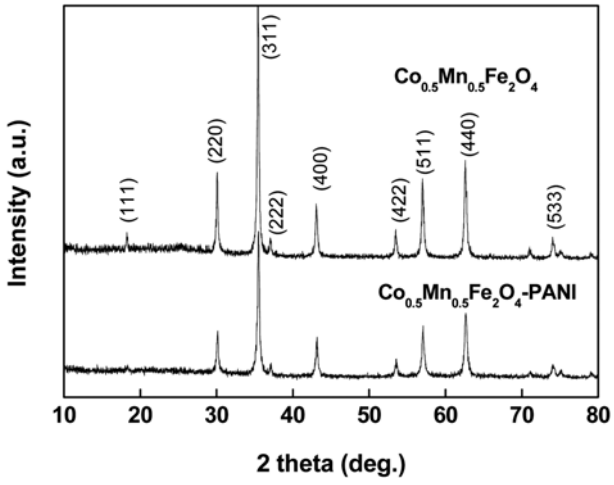

Fig. 3. XRD Patterns of hollow $Co_{0.5}Mn_{0.5}Fe_2O_4$ and $Co_{0.5}Mn_{0.5}Fe_2O_4$-PANI nanofibers.

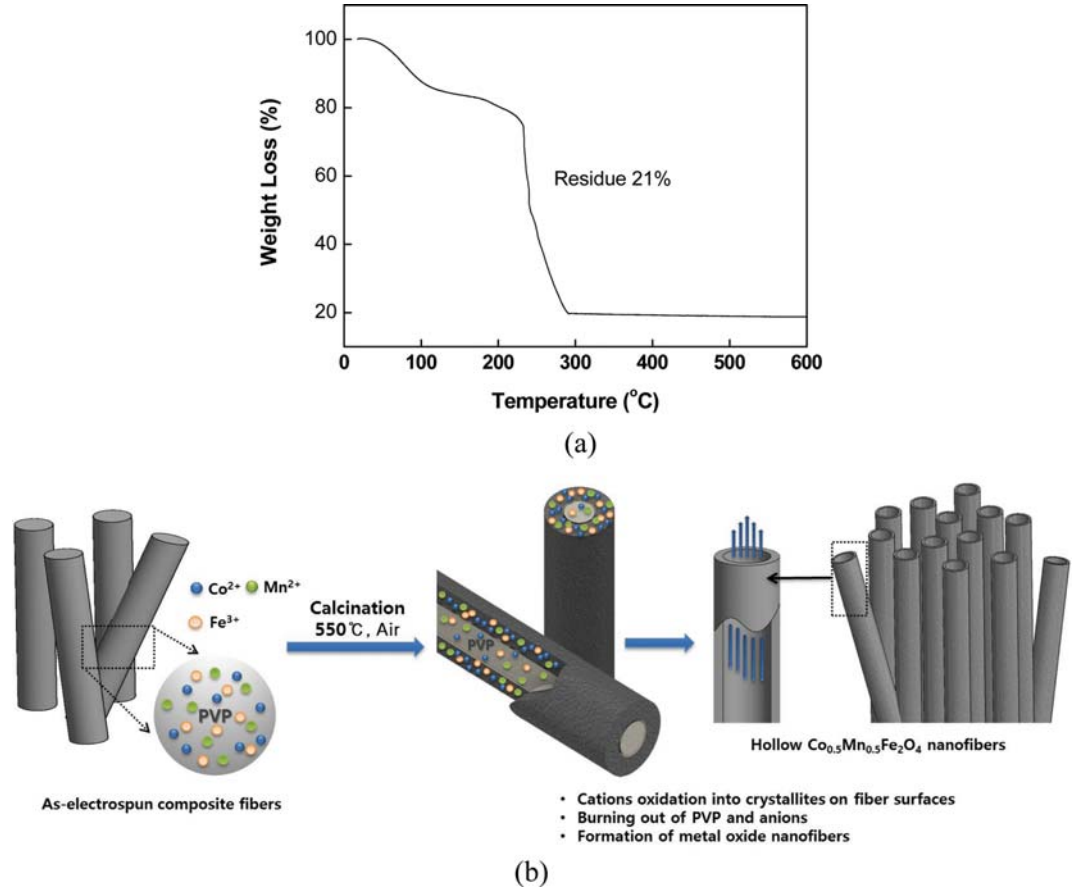

Fig. 4. (a) TGA curves of as-spun composite fibers and (b) the schematic diagram of formation for hollow $Co_{0.5}Mn_{0.5}Fe_2O_4$ nanofibers.

(533) planes of Co-Mn ferrite spinel structures with face centered cubic phase [28,29]. The diffraction peaks of hollow $Co_{0.5}Mn_{0.5}Fe_2O_4$-PANI nanofibers slightly decrease compared to hollow $Co_{0.5}Mn_{0.5}Fe_2O_4$ fibers with the strong crystallinity, implying PANI coating on the surface of hollow $Co_{0.5}Mn_{0.5}Fe_2O_4$ fibers [30,31].

3. Mechanism of Hollow $Co_{0.5}Mn_{0.5}Fe_2O_4$ Nanofibers

Fig. 4 shows the thermogravimetric analysis (TGA) of electrospun PVP/$Co_{0.5}Mn_{0.5}Fe_2O_4$ precursors and the schematic diagram of formation for hollow $Co_{0.5}Mn_{0.5}Fe_2O_4$ nanofibers. As for Fig. 4(a), the initial weight loss of 16% is due to the water evaporation up to 100 °C. The second weight loss of 25% was caused by the nitrate decomposition in metal precursors ranging from 190 to 240 °C, giving rise to the shrinkage of the nanofibers. The third weight loss is due to the PVP removal, inducing the hollow core in the range of 250 to 400 °C, as shown in TEM images of Fig. 2(a) and (b). The residue of hollow $Co_{0.5}Mn_{0.5}Fe_2O_4$ nanofibers was 21% after calcining in air at 550 °C for 2 h. Fig. 4(b) shows the fabricating process of hollow $Co_{0.5}Mn_{0.5}Fe_2O_4$ nanofibers prepared by electrospinning and thermal process. The composite solution mixed metal precursors with PVP is composed of PVP/cobalt nitrate, PVP/manganese nitrate, and PVP/iron nitrate, generating physical interaction of Co^{2+}, Mn^{2+} and Fe^{3+} with the oxygen groups of PVP. In the process of calcination, three nitrates in PVP/metal precursor nanofibers begin to decompose from the surface of as-prepared nanofibers to form $Co_{0.5}Mn_{0.5}Fe_2O_4$, but three metal precursors in the interior portion of hollow fibers are hard to decompose due to the deficiency of oxygen. Afterwards, three metal precursors present in the interior region are easily diffused towards the outer surface of nanofibers caused by the concentration difference with distance, engendering that the outer surface of nanofibers is rich with PVP/metal precursors, whereas the interior of nanofibers is full of PVP template [32-35]. The PVP in a series of calcination process is decomposed generating hollow core, which creates hollow core-$Co_{0.5}Mn_{0.5}Fe_2O_4$ shell morphology. Another thermogravimetric analysis of PANI, hollow $Co_{0.5}Mn_{0.5}Fe_2O_4$ nanofibers and $Co_{0.5}Mn_{0.5}Fe_2O_4$-PANI nanofibers is given in Fig. 5. As to PANI, the first weight loss up to ~100 °C is owning to the residual water. The second weight loss ranging from 250-630 °C is coincided with the decomposition of PANI chains. The content of hollow $Co_{0.5}Mn_{0.5}Fe_2O_4$ nanofibers remains ~100% due to the existence of metal oxide. As for hollow $Co_{0.5}Mn_{0.5}Fe_2O_4$-PANI nanofibers, the first weight loss up to ~100 °C is attributed to the residual water evaporation. The second weight loss ranging from 270-500 °C is caused by the PANI decomposition. In the calcination process of 500 °C or more, the hollow $Co_{0.5}Mn_{0.5}Fe_2O_4$ nanofibers still remains ~43% generating $Co_{0.5}Mn_{0.5}Fe_2O_4$ shell.

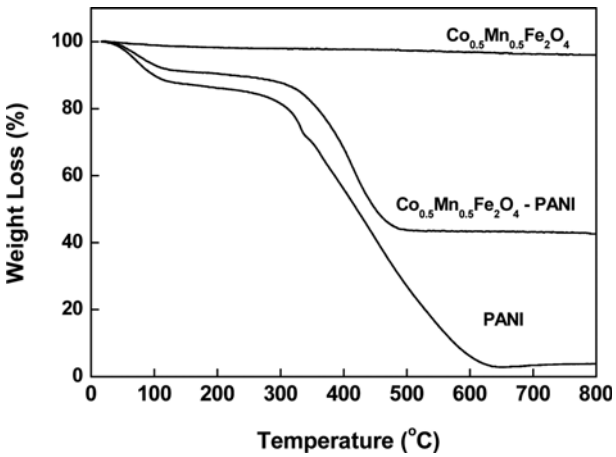

Fig. 5. TGA curves of PANI, hollow $Co_{0.5}Mn_{0.5}Fe_2O_4$ and hollow $CoMnFe_2O_4$-PANI nanofibers.

4. Pore Size Distribution of Hollow $Co_{0.5}Mn_{0.5}Fe_2O_4$ and $Co_{0.5}Mn_{0.5}Fe_2O_4$-PANI Nanofibers

Fig. 6 shows nitrogen adsorption-desorption isotherms and pore size distributions of $Co_{0.5}Mn_{0.5}Fe_2O_4$ and hollow $Co_{0.5}Mn_{0.5}Fe_2O_4$-PANI nanofibers. All samples represent the hysteresis behavior normalized with the typical IV pattern owning to meso/macroporous structures with hollow nanofibers. As for Fig. 6(a), the hollow $Co_{0.5}Mn_{0.5}Fe_2O_4$ nanofibers begin to observe adsorption hysteresis at high relative pressure of ~0.8, while the hollow $Co_{0.5}Mn_{0.5}Fe_2O_4$-PANI nanofibers start to show at low relative pressure of ~0.45 caused by PANI coating over hollow $Co_{0.5}Mn_{0.5}Fe_2O_4$ nanofibers. The pore size distributions evaluated by the BJH method for the hollow $Co_{0.5}Mn_{0.5}Fe_2O_4$ and $Co_{0.5}Mn_{0.5}Fe_2O_4$-PANI nanofibers are shown in Fig. 6(b). The pore characteristics of both samples are divided into small mesopores from 2-10 nm, intermediate meso-

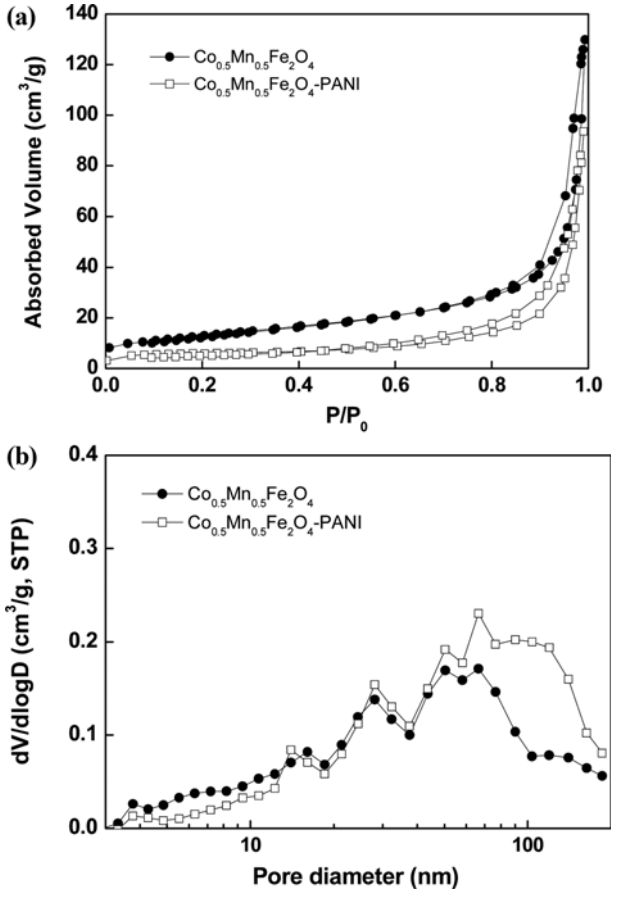

Fig. 6. (a) Nitrogen adsorption-desorption isotherms and (b) pore size distributions of hollow $Co_{0.5}Mn_{0.5}Fe_2O_4$ and $Co_{0.5}Mn_{0.5}Fe_2O_4$-PANI nanofibers.

Table 1. Pore characteristics of hollow $Co_{0.5}Mn_{0.5}Fe_2O_4$ and $Co_{0.5}Mn_{0.5}Fe_2O_4$-PANI nanofibers

Sample	BET surface area (m^2/g)	Total pore volume (cm^3/g)	Micropore volume (cm^3/g)	Mesopore avg. dia. (nm)
$Co_{0.5}Mn_{0.5}Fe_2O_4$	21.9	0.144	<0.01	26.2
$Co_{0.5}Mn_{0.5}Fe_2O_4$-PANI	20.8	0.176	<0.01	35.4

pores from 10-20 nm, large mesopores from 20-50 nm, and macropores from 50-120 nm, possessing mesoporosity and macroporosity nearly without microporosity, In detail, the mesopore region from 2-50 nm for both samples is generated by a similar pattern, but the macropore region from 50-120 nm for $Co_{0.5}Mn_{0.5}Fe_2O_4$-PANI is well-developed compared to $Co_{0.5}Mn_{0.5}Fe_2O_4$ caused by the better macroporous morphology of the interlayers of nanofibers coated with entangled PANI. The PANI coating as the second shell on the rough surface of hollow $Co_{0.5}Mn_{0.5}Fe_2O_4$ nanofibers as the first shell stimulates the adsorption of methyl orange, promotes the electron transfer through 1D pathway, provides abundant photocatalytic sites due to the formation of excellent porous morphology, and makes it recover magnetically separable photocatalysts. The pore characterization of hollow $Co_{0.5}Mn_{0.5}Fe_2O_4$ and $Co_{0.5}Mn_{0.5}Fe_2O_4$-PANI nanofibers is shown in Table 1. Both samples retain meso/macroporous morphology nearly without micropore volume. The specific surface area, mean pore diameter, and total pore volume of hollow $Co_{0.5}Mn_{0.5}Fe_2O_4$ nanofibers are 21.9 $m^2\ g^{-1}$, 26.2 nm, and 0.144 $cm^3\ g^{-1}$, while those of hollow $Co_{0.5}Mn_{0.5}Fe_2O_4$-PANI nanofibers are 20.8 $m^2\ g^{-1}$, 35.4 nm, and 0.176 $cm^3\ g^{-1}$, respectively. The surface area of hollow $Co_{0.5}Mn_{0.5}Fe_2O_4$-PANI nanofibers is slightly less than that of hollow $Co_{0.5}Mn_{0.5}Fe_2O_4$ one due to the pore blockage of PANI coating. Meantime, the hollow $Co_{0.5}Mn_{0.5}Fe_2O_4$-PANI nanofibers illustrate better mesoporous morphology compared to hollow $Co_{0.5}Mn_{0.5}Fe_2O_4$ nanofiber owning to PANI entanglement by PANI coating on the surface of hollow $Co_{0.5}Mn_{0.5}Fe_2O_4$ nanofiber. As a result, hollow $Co_{0.5}Mn_{0.5}Fe_2O_4$-PANI nanofibers promote the facile capture of visible light, leading to the fast photodegradation of MO dye.

5. Optical Absorption Properties and Adsorption Capacity of MO for Hollow $Co_{0.5}Mn_{0.5}Fe_2O_4$, PANI and $Co_{0.5}Mn_{0.5}Fe_2O_4$-PANI Nanofibers

The excellent photocatalysis for MO decomposition is deeply related to the ample absorption of visible light and the abundant adsorption of MO dye for the photocatalysts [36]. Fig. 7(a) shows the UV-vis diffuse reflectance spectra for $Co_{0.5}Mn_{0.5}Fe_2O_4$ and hollow $Co_{0.5}Mn_{0.5}Fe_2O_4$-PANI nanofibers. As for hollow $Co_{0.5}Mn_{0.5}Fe_2O_4$ nanofibers, high absorption intensity is observed in the UV light of less than 380 nm, whereas declining absorption intensity is detected in the visible light region of 380-800 nm. On the other hand, the PANI as a promising sensitizer shows the facile absorption over both UV and visible region caused by its conjugated pi-electron system, which results in high mobility of charge carriers. Likewise, the hollow $Co_{0.5}Mn_{0.5}Fe_2O_4$-PANI nanofibers with heterojunction exhibit excellent absorption intensity throughout the entire region of UV/visible spectrum. The results show that the hollow $Co_{0.5}Mn_{0.5}Fe_2O_4$ nanofibers only separate the holes and electrons in the UV region, whereas the heterojunction structure in which the hollow $Co_{0.5}Mn_{0.5}Fe_2O_4$ nanofibers surface is coated with PANI nanoparticles induces photoinduced charge separation easily throughout the UV-vis region. As a result, the heterostructured $Co_{0.5}Mn_{0.5}Fe_2O_4$-PANI hollow nanofibers with meso-/macroporous structures induce efficient quantum confinement and active photocatalysis by easily harvesting the incident beam, facilitating the mass transfer of MO dye, preventing the recombination of the photogenerated carrier, and leading to the easy recovery of photocatalysts due to the excellent magnetic property. Fig. 7(b) represents adsorption capacity of MO dye according to the time for the hollow $Co_{0.5}Mn_{0.5}Fe_2O_4$ and $Co_{0.5}Mn_{0.5}Fe_2O_4$-PANI nanofibers as photocatalysts. The $Co_{0.5}Mn_{0.5}Fe_2O_4$ consists of 1D hollow nanofibers with hollow core and $Co_{0.5}Mn_{0.5}Fe_2O_4$ shell, whereas the $Co_{0.5}Mn_{0.5}Fe_2O_4$-PANI with a triple layer is comprised of 1D hollow nanofibers with hollow core and shell coated with PANI on the surface of $Co_{0.5}Mn_{0.5}Fe_2O_4$. The $Co_{0.5}Mn_{0.5}Fe_2O_4$ photocatalyst without PANI is hard to adsorb MO dye because there is no functional group. On the other hand, the $Co_{0.5}Mn_{0.5}Fe_2O_4$-PANI photocatalyst is completely saturated within 20 min, representing the adsorption capacity of 0.054 mg MO per 1 mg photocatalyst. In detail, the adsorption capacity of MO per 1 mg photocatalyst represents 0.048 mg in 5 min, and 0.05 mg in

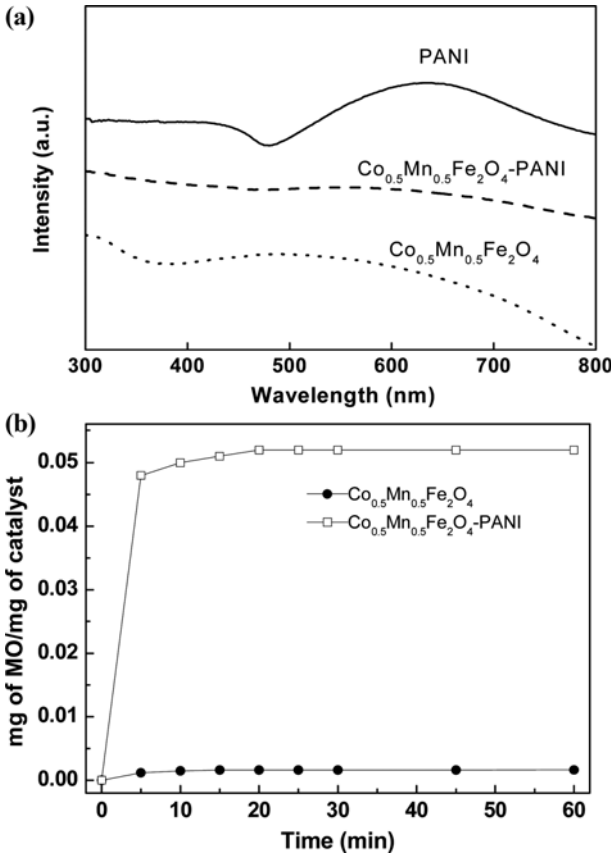

Fig. 7. (a) UV-vis spectra and (b) adsorption capacity with time for hollow $Co_{0.5}Mn_{0.5}Fe_2O_4$ and $Co_{0.5}Mn_{0.5}Fe_2O_4$-PANI nanofibers as photocatalysts.

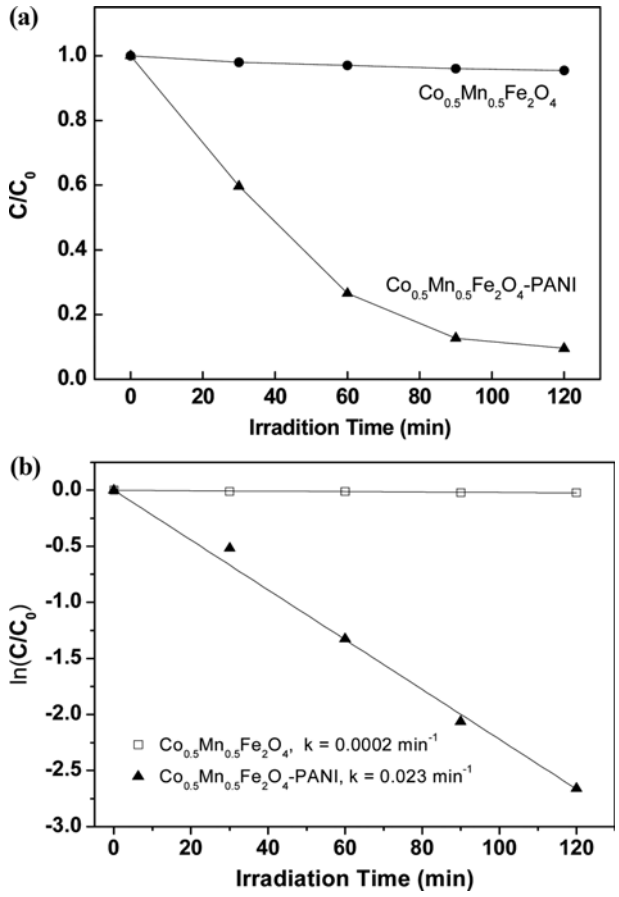

Fig. 8. (a) Photodegradation and (b) kinetic linear simulation curves of MO for hollow $Co_{0.5}Mn_{0.5}Fe_2O_4$ and $Co_{0.5}Mn_{0.5}Fe_2O_4$-PANI nanofibers under visible-light irradiation.

10 min. This originates from (1) numerous meso/macroporous structure generated by 1D hollow nanofibers with hollow core and a triple PANI/$Co_{0.5}Mn_{0.5}Fe_2O_4$/PANI shell, and (2) the molecular interaction between positively charged backbone of PANI and negatively charged MO dye. Both mesoporous structure and effective interaction created by PANI enable MO dye to adsorb better by enhancing the rate of mass transfer.

6. Photodegradation Properties of Hollow $Co_{0.5}Mn_{0.5}Fe_2O_4$-PANI Nanofibers

Fig. 8(a) shows the photodegradation of MO dye for $Co_{0.5}Mn_{0.5}Fe_2O_4$ and $Co_{0.5}Mn_{0.5}Fe_2O_4$-PANI under visible-light irradiation at ambient condition. As to $Co_{0.5}Mn_{0.5}Fe_2O_4$, the photodegradation efficiency of MO dye shows below 5% under visible-light irradiation owing to the inactivity by the restriction of wide band gap. As for $Co_{0.5}Mn_{0.5}Fe_2O_4$-PANI, the photodegradation efficiency of MO is steeply improved, showing 80% in 60 min, 90% in 90 min, and 92% in 120 min. The exceptional photodegradation of the MO dye by tremendous photocatalytic activity of $Co_{0.5}Mn_{0.5}Fe_2O_4$-PANI results from (1) the facile capture of visible light by hollow core/double shell nanofibers with large surface area generating quantum confinement effect, (2) meso/macroporous nanostructures by 1D hollow nanofibers with large aspect ratio promoting both mass transfer and electron transfer, (3) 1D heterostructured $Co_{0.5}Mn_{0.5}Fe_2O_4$-polyaniline system promoting charge separation, (4) easy adsorption of MO for ample photodegradation by the interior and outer surfaces among the nanofibers with hollow core-triple shell nanostructures, and (5) easy photocatalyst recovery with exceptional magnetically separable property by 1D hollow nanofibers with heterostructured system. The comparison of photodegradation efficiency for other photocatalysts is summarized in Table 2 [37-43]. Fig. 8(b) illustrates the kinetic simulation of MO dye for the hollow $Co_{0.5}Mn_{0.5}Fe_2O_4$ and $Co_{0.5}Mn_{0.5}Fe_2O_4$-PANI nanofibers under visible-light irradiation. The kinetics of MO photodegradation for hollow $Co_{0.5}Mn_{0.5}Fe_2O_4$-PANI nanofiber under visible-light irradiation is defined by pseudo-first order reaction as follows.

$$-\ln (C/C_o)=kt$$

where k is defined as the kinetic rate constant (min^{-1}), C_o represents the initial concentration of MO, and C signifies the concentration of MO at a certain time (t). The kinetic rate constants (k) calculated from the ratio by logarithmic scale with irradiation time are shown in Fig. 8(b). The kinetic rate constant (k) of $Co_{0.5}Mn_{0.5}Fe_2O_4$ nanofibers is 0.0002 min^{-1}, while that of $Co_{0.5}Mn_{0.5}Fe_2O_4$-PANI fibers is 0.023 min^{-1}. So, the kinetic rate of $Co_{0.5}Mn_{0.5}Fe_2O_4$-PANI fibers is 115-times faster than that of $Co_{0.5}Mn_{0.5}Fe_2O_4$ nanofibers, implying excellent photocatalytic activity as a photocatalyst with the morphological characteristics of the hollow nanofiber coated with PANI.

Fig. 9 shows the cycling stability of $Co_{0.5}Mn_{0.5}Fe_2O_4$-PANI photocatalyst according to the repeated experiment under visible-light irradiation. The photodegradation of MO dye was carried out three times. After each photodegradation experiment, the $Co_{0.5}Mn_{0.5}Fe_2O_4$-PANI photocatalyst was recovered by using magnets, and it was

Table 2. Photocatalytic performances of other metal oxide nanocomposites

Samples	Lights	Dyes	Photodegradation (%)	Irradiation time (h)	Reference
$CoFe_2O_4$-graphene	Visible	MO	70	4	35
$CoFe_2O_4$-PANI composite	Visible	MO	80	8	6
$CoFe_2O_4$-PANI composite	UV	MO	87	4	36
TiO_2-$CoFe_2O_4$-PANI	Visible	MO	80	3	37
$CoFe_2O_4$-RGO	Visible	MO	40	3	38
$CoFe_2O_4$-Fe_3O_4 composite	UV	MO	93	5	39
$CoFe_2O_4$-BiOI	Visible	MO	80	4	40,41
$Co_{0.5}Mn_{0.5}Fe_2O_4$-PANI	Visible	MO	91	2	This study

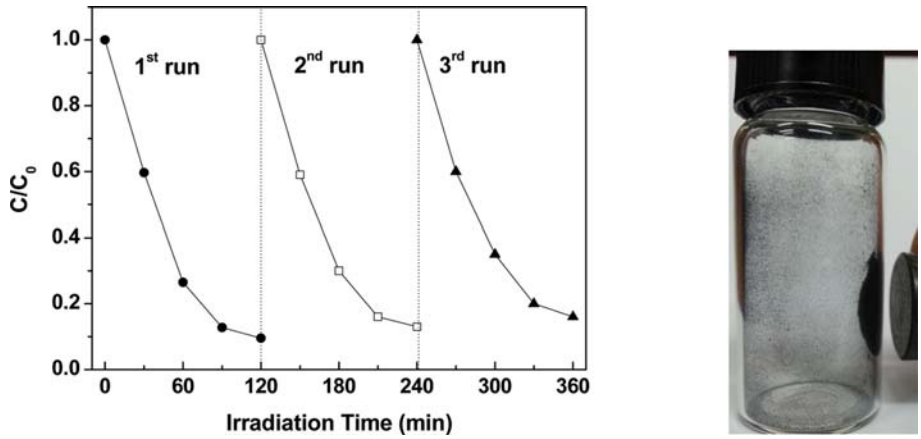

Fig. 9. Cycling runs in photocatalytic degradation efficiency of MO for hollow $Co_{0.5}Mn_{0.5}Fe_2O_4$-PANI nanofibers under visible-light irradiation.

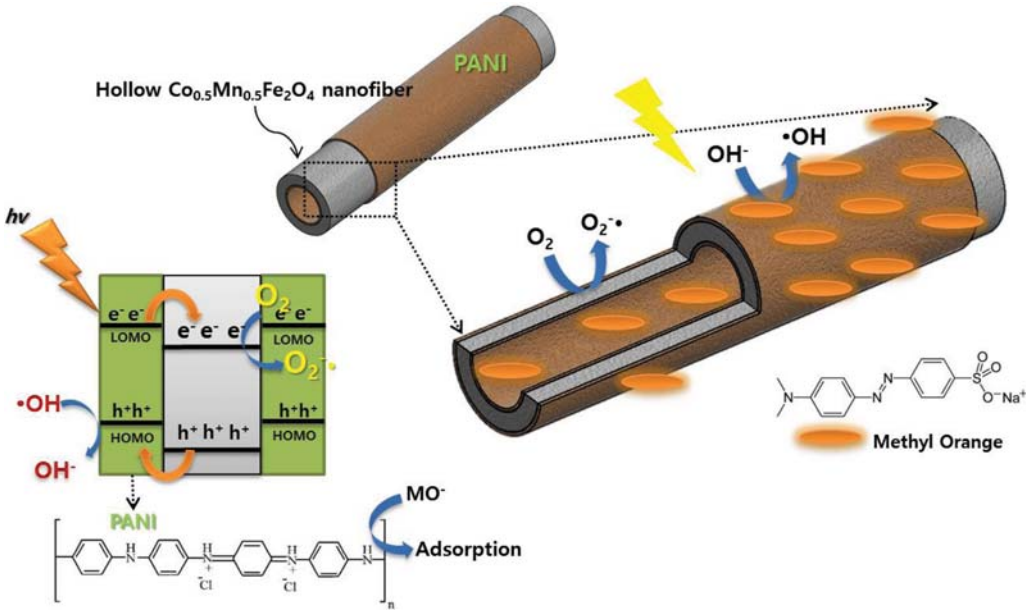

Fig. 10. Schematic diagram of photodegradation of MO dye for hollow $Co_{0.5}Mn_{0.5}Fe_2O_4$-PANI nanofibers under visible-light irradiation.

reused after cleaning several times. The hollow $Co_{0.5}Mn_{0.5}Fe_2O_4$ nanofibers exhibit almost the same photocatalytic property even after three cycles under visible-light irradiation, indicating that hollow $Co_{0.5}Mn_{0.5}Fe_2O_4$ nanofibers represent excellent photodegradation efficiency and superior stability as a photocatalyst. The hollow $Co_{0.5}Mn_{0.5}Fe_2O_4$-PANI nanofibers remarkably improve the separation of electron-hole pairs by numerous heterojunctions, guaranteeing abundant photocatalytic active sites by large surface area with mesoporous and macroporous morphology, and facilitating mass transfer by the sufficient absorption of MO dye.

Fig. 10 is a schematic diagram of MO dye photodegradation for hollow $Co_{0.5}Mn_{0.5}Fe_2O_4$-PANI nanofibers under visible-light irradiation. The photocatalytic reaction of hollow nanofibers is predicted as follows. First, when visible light is irradiated on the PANI of hollow $Co_{0.5}Mn_{0.5}Fe_2O_4$-PANI nanofibers, electrons move from the valence band to the conduction band, and then the holes are generated in the valence band. Thus, an electron-hole pair (exciton) is formed in PANI as the electron donor by visible light absorption. Second, the electrons present in LUMO of PANI are transferred to the conduction band of $Co_{0.5}Mn_{0.5}Fe_2O_4$ and at the same time holes are formed in $Co_{0.5}Mn_{0.5}Fe_2O_4$. Third, the hole formed in $Co_{0.5}Mn_{0.5}Fe_2O_4$ is inserted into the HOMO of PANI. Finally, the heterojunction structure of hollow $Co_{0.5}Mn_{0.5}Fe_2O_4$-PANI nanofibers decomposes the MO dye by producing superoxide anion radicals, hydroxyl radicals, and holes through the separation of electron-hole [44]. The heterostructured $Co_{0.5}Mn_{0.5}Fe_2O_4$-PANI hollow nanofibers with large surface area lead to excellent photodegradation by enhanced photoinduced separation, create photocatalytically active sites suitable for facile photocatalysis, and promote photokinetic reaction by the superb absorption of visible light.

CONCLUSIONS

Hollow $Co_{0.5}Mn_{0.5}Fe_2O_4$-PANI nanofibers were fabricated through

sequential electrospinning, heat treatment, and chemical polymerization of PANI. The 1D hollow $Co_{0.5}Mn_{0.5}Fe_2O_4$-PANI nanofibers lead to a large surface area with meso/macroporous morphology, abundant heterojunction, excellent capture of visible light, and sufficient adsorption of MO dye with negatively charged groups or electron-rich groups. As a result, hollow $Co_{0.5}Mn_{0.5}Fe_2O_4$-PANI nanofibers exhibit excellent photocatalytic activity and exceptional photodegradation efficiency of MO dyes by promoting the transfer of photoinduced carrier and separation of electron-hole pair. Also, the magnetic property of hollow $Co_{0.5}Mn_{0.5}Fe_2O_4$-PANI nanofibers induces excellent recovery after photodegradation process. On the other hand, hollow $Co_{0.5}Mn_{0.5}Fe_2O_4$ nanofibers without PANI exhibit easy recombination of electron-hole pairs, giving rise to low photocatalytic efficiency under visible-light irradiation.

ACKNOWLEDGEMENT

This work was supported by the National Research Foundation of Korea (NRF) grant funded by the Korea government (MSIP) (No. 2017R1D1A3B03029996).

REFERENCES

1. E. Casbeer, V. K. Sharma and X.-Z. Li, *Sep. Purif. Technol.*, **87**(5), 1 (2012).
2. G. Padmapriya, A. Manikandan, V. Krishnasamy, S. K. Jaganathan and S. A. Antony, *J. Mol. Struct.*, **1119**, 39 (2016).
3. S.-Q. Liu, B. Xiao, L.-R. Feng, S.-S. Zhou, Z.-G. Chen, C.-B. Liu, F. Chen, Z.-Y. Wu, N. Xu, W.-C. Oh and Z.-D. Meng, *Carbon*, **64**, 197 (2013).
4. G. Mathubala, A. Manikandan, S. A. Antony and P. Ramar, *Nanosci. Nanotech. Lett.*, **8**(5), 375 (2016).
5. C. Barathiraja, A. M. U. Mohideen and S. Jayasree, *Advan. Sci. Eng. Med.*, **8**(12), 968 (2016).
6. P. Xiong, Q. Chen, M. Y. He, X. Q. Sun and X. Wang, *J. Mater. Chem.*, **22**(34), 17485 (2012).
7. S. H. Sun, H. Zeng, D. B. Robinson, S. Raoux, P. M. Rice, S. X. Wang and G. X. Li, *J. Am. Chem. Soc.*, **126**(1), 273 (2004).
8. K. J. Kim, H. K. Kim, Y. R. Park and J. Y. Park, *J. Magn. Magn. Mater.*, **304**, e106 (2006).
9. P. Chitra, A. Muthusamy and R. Jayaprakash, *J. Magn. Magn. Mater.*, **396**, 113 (2015).
10. G. Padmapriya, A. Manikandan, V. Krishnasamy, S. K. Jaganathan and S. A. Antony, *J. Mol. Struct.*, **1119**, 39 (2016).
11. J. Hua, Y, Liu, L. Wang, M. Feng, J. L. Zhao and H. B. Li, *J. Magn. Magn. Mater.*, **402**, 166 (2016).
12. S. M. Ramay, M. Saleem, S Atiq, S. A. Siddiqi, S. Naseem and M. S. Anwar, *Bull. Mater. Sci.*, **34**(7), 1415 (2011).
13. X. Y. Zhang, J. Q. Qin, Y. N. Xue, P. F. Yu, B. Zhang, L. M. Wang and R. P. Liu, *Sci. Rep.*, **4**, 4596 (2014).
14. X. F. Lu, C. Wang and Y. Wei, *Small*, **5**(21), 2349 (2009).
15. Z. Q. Su, J. W. Ding and G. Wei, *RSC Adv.*, **4**, 52598 (2014).
16. S.-H. Park and W.-J. Lee, *Sci. Rep.*, **5**, 9754 (2015).
17. S.-H. Park and W.-J. Lee, *RSC Adv.*, **5**, 23548 (2015).
18. Y.-W. Ju, J.-H. Park, H.-R. Jung, S.-J. Cho and W.-J. Lee, *Compos. Sci. Technol.*, **68**(7-8), 1704 (2008).
19. L. Wang, G. R. Yang, S. J. Peng, J. N. Wang, D. X. Ji, W. Yan and S. R. Ramakrishna, *Int. J. Hydrogen Energy*, **42**, 2558 (2017).
20. G. Panthi, M. Park, H.-Y. Kim, S.-Y. Lee and S.-J. Park, *J. Ind. Eng. Chem.*, **21**, 26 (2015).
21. P. P. Dasa, A. Roy, M. Tathavadekar and P. S. Devi, *Appl. Catal. B: Environ.*, **203**, 692 (2017).
22. H. Zhang, R. L. Zong, J. C. Zhao and Y. F. Zhu, *Environ. Sci. Technol.*, **42**(10), 3803 (2008).
23. K. R. Reddy, M. Hassan and V. G. Gomes, *Appl. Catal. A: Gen.*, **489**, 1 (2015).
24. K. N. Kim, H.-R. Jung and W.-J. Lee, *J. Photochem. Photobiol. A: Chem.*, **321**(1), 257 (2016).
25. G. Z. Liao, S. Chen, X. Quan, Y. B. Zhang and H. M. Zhao, *Appl. Catal. B: Environ.*, **102**, 126 (2011).
26. N. N. Bahrudin, M. A. Nawi and W. I. N. W. Ismail, *Korean J. Chem. Eng.*, **35**(7), 1450 (2018).
27. U. Kurtan, Y. Junejo, B. Unal and A. Baykal, *J. Inorg. Organomet. Polym.*, **23**, 1086 (2013).
28. A. Hankeem, G. Murtaza, I. Ahmad, P. Mao, X. Guohua, M. T. Farid, M. Kanwal, G. Mustafa, M. Hussain and M. Ahmad, *Digest J. Nanomater. Biostruct.*, **11**, 149 (2016).
29. O. Vozniuk, C. Bazzo, S. Albonetti, N. Tanchoux, F. Bosselet, J.-M. M. Millet, F. D. Renzo and F. Cavani, *Chem. Cat. Chem.*, **9**, 2219 (2017).
30. A. Pant, R. Tanwar, B. Kaur and U. K. Mandal, *Sci. Rep.*, **8**, 14 (2018).
31. K. N. Kim, H.-R. Jung and W.-J. Lee, *Sci. Adv. Mater.*, **9**(11), 1993 (2017).
32. X. Xia, X. J. Dong, Q. F. Wei, Y. B. Cai and K. Y. Lu, *Express Polymer Lett.*, **6**(2), 169 (2012).
33. S. S. Sainudeen, L. B. Asok, A. Varghese, A. S. Nair and G. Krishnan, *RSC Adv.*, **7**(56), 35160 (2017).
34. S. H. Wei, M. H. Zhou and W. P. Du, *Sensor. Actuat. B*, **160**, 753 (2011).
35. T. T. Wang, S. Y. Ma, L. Cheng, J. Luo, X. H. Jiang and W. X. Jin, *Sensor. Actuat. B*, **216**, 212 (2015).
36. L. Yang, Y. An, B. Dai, X. H. Guo, Z. Y. Liu and B. H. Peng, *Korean J. Chem. Eng.*, **34**(2), 476 (2017).
37. Y. S. Fu, H. Q. Chen, X. Q. Sun and X. Wang, *Appl. Catal. B: Environ.*, **111**, 280 (2012).
38. J. A. Khan, M. Qasim, B. R. Singh, S. Singh, M. Shoe, W. Khan, D. Das and A. H. Naqvi, *Spectrochim. Acta, Part A: Mol. Biomol. Spectrosc.*, **109**, 313 (2013).
39. C. J. Leng, J. H. Wei, Z. Y. Liu, R. Xiong, C. X. Pan and J. Shi, *J. Nanopart. Res.*, **15**, 1643 (2013).
40. G. Y. He, J. J. Ding, J. G. Zhang, Q. L. Hao and H. Q. Chen, *Ind. Eng. Chem. Res.*, **54**, 2862 (2015).
41. D. Mishra, K. K. Senapati, C. Borgohain and A. Perumal, *J. Nanotech.*, **323145**, 1 (2012).
42. Y. I. Choi, Y.-I. Kim, D. W. Cho, J.-S. Kang, K. T. Leung and Y. K. Sohn, *RSC Adv.*, **5**, 79624 (2015).
43. S. Singh, R. Sharma and M. Khanuja, *Korean J. Chem. Eng.*, **35**(10), 1955 (2018).
44. S. Sehar, I. Naz, I. Perveen and S. Ahme, *Korean J. Chem. Eng.*, **36**(1), 56 (2019).